communications physics

ARTICLE

https://doi.org/10.1038/s42005-023-01510-8 OPEN

# Effect of vessel compression on blood flow in microvascular networks and its implications for tumour tissue hypoxia

Romain Enjalbert [1], Timm Krüger [2,4]✉ & Miguel O. Bernabeu [1,3,4]✉

The tumour microenvironment is abnormal and one of its consequences is that blood vessels are compressed. Vessel compression correlates with reduced survival rates, while decompression of vessels improves tissue oxygenation as well as increases survival rates. Vessel compression contributes, at a single vascular bifurcation, to the increase of heterogeneity of red blood cell (RBC) transport. However, the effect that vessel compression has at a network level is unknown. This work numerically investigates the effect of vessel compression on RBC transport in microvascular networks. The key findings are that vessel compression both reduces the average haematocrit, and increases haematocrit heterogeneity, in vessels in the network. The mechanisms for these changes in haematocrit distribution are unravelled, and a parameter sweep shows that networks with lower inlet haematocrits are more susceptible to haemodilution from vessel compression over a wide range of compressed fraction of a network. These findings provide a theoretical underpinning for the link between vessel compression and tumour tissue hypoxia.

[1] Centre for Medical Informatics, Usher Institute, The University of Edinburgh, Edinburgh EH16 4UX, UK. [2] School of Engineering, Institute for Multiscale Thermofluidics, The University of Edinburgh, Edinburgh EH9 3FD, UK. [3] The Bayes Centre, The University of Edinburgh, Edinburgh EH8 9BT, UK. [4] These authors contributed equally: Timm Krüger, Miguel O. Bernabeu. ✉email: timm.krueger@ed.ac.uk; miguel.bernabeu@ed.ac.uk

Solid tumours have an abnormal microenvironment, leading to tumour tissue hypoxia[1]. Hypoxia is an undesirable trait as it is associated with reduced patient survival rates through two separate mechanisms: increased tumour aggressiveness and resistance to tumour treatment[2,3].

More recent therapeutic avenues have not translated to expected patient benefit, and the presence of hypoxia is one of the causes for that[4–6]. Blood vessel compression is one specific tumour microenvironment abnormality[7–9]. Previous work correlates the degree of vessel compression with reduced survival rates[8] and shows that pharmacologically decompressing vessels improves survival rates[10]. Furthermore, vessel compression is associated with tissue hypoxia as well as increased oxygen heterogeneity in the tissue[10].

The cause for increased hypoxia and increased oxygen heterogeneity due to vessel compression has not been fully elucidated[10]. At microvascular bifurcations, red blood cells (RBCs) heterogeneously partition to the child branches due to the finite size of RBCs[11,12]. Our previous work has shown that another structural abnormality, reduced interbifucation distance, changes the partitioning of the RBCs to the child branches at individual bifurcations, leading to increased tissue oxygen at a network level[13]. We previously showed that, at a single vascular bifurcation, vessel compression leads to a more heterogeneous partitioning of RBCs in the child branches of a bifurcation[14]. Given RBCs' role in the transport of oxygen in blood[15], it follows that oxygen transport is altered too. Previous work suggests that increased resistance to blood flow due to vessel compression leads to reduced perfusion to the blood vessels[16,17]. However, how vessel compression affects haematocrit in blood vessels at a network level is unknown, nor has it been elucidated whether it drives tissue hypoxia.

In the current study, we find that vessel compression both reduces the average haematocrit, and increases haematocrit heterogeneity, in vessels in the network. We further show that networks with lower inlet haematocrits are more susceptible to haemodilution from vessel compression. These findings provide a theoretical underpinning for the link between vessel compression and tumour tissue hypoxia.

## Results

**Adapting the reduced-order model for compressed vessels**. To model the partitioning of RBCs in compressed vessels at a network level, we adapt an existing reduced-order model, developed by Pries et al.[18,19], to account for vessel compression. Figure 1a shows a flow chart illustrating the method we used to update the reduced-order model. We choose to adapt Pries' model due to its robustness and ubiquity in the literature[18].

We initially demonstrate that the term that needs adapting in the model is $X_0$ (see Supplementary Note 1 for details on $X_0$). We run a series of resolved RBC simulations (see Fig. 1b and c), varying the flow ratio in a bifurcation geometry with 33 μm branches with compression before the bifurcation (the parent branch is compressed into an elliptical vessel whose cross-section has an aspect ratio of 4.26, while preserving the vessel perimeter of the circular cross-section, as per ref. [14]) and an inlet haematocrit of 20%. We plot the results as a plasma skimming curve, Fig. 1d, and show that by adapting $X_0$ we obtain a close fit to the data generated in compressed vessels.

Supported by this evidence, we set out to find a new functional form for $X_0$ for cases when vessels are compressed. We fully resolve a set of 20 bifurcations with HemeLB simulations (see Supplementary Note 2 and Supplementary Table 1). The flow ratios, haematocrit values, and diameters in Supplementary Table 1 were taken from the diverging bifurcations in the network that will be used (see Fig. 2a) to be representative of the bifurcations that the updated phase separation model will resolve. The haematocrit and flow ratio in these bifurcations were obtained by solving the Poiseuille flow through the entire network using the standard phase separation model for RBC partitioning[18,19].

Next, we need to find the values of $X_0$ for the results of these simulations that match the child branch haematocrit values from the fully resolved simulations. We analytically invert the main equation of the Pries model to make $X_0$ the subject of the equation

$$X_0 = \frac{FQ_B + FQ_B e^{\alpha} - e^{\alpha}}{1 - e^{\alpha}} \tag{1}$$

where $FQ_B$ is the fraction of blood flowing to a child branch and $\alpha$ is defined as

$$\alpha = \frac{\mathrm{logit}\,(FQ_E) - A}{B} \tag{2}$$

where $FQ_E$ is the fraction of RBC flowrate flowing to a child branch and $A$ and $B$ are terms defined in the original empirical model[18,19].

We calculate the updated value of $X_0$ for compressed vessels, $X_0^c$, from Eq. (1) and $FQ_E$ values from Supplementary Table 1. Figure 1e and f show that $X_0^c$ is inversely proportional to $D$ and decreases linearly with $H$. Therefore, we keep the original functional form, and update the pre-factor:

$$X_0^c = C\frac{1 - H_D}{D_P} \tag{3}$$

where $H_D$ is the discharge haematocrit in the parent branch, $D_P$ is the diameter of the parent branch, and $C$ is the pre-factor to be determined for the new functional form for $X_0^c$. We use a non-linear least-squares method to fit $C$ and obtain a value of 4.16, yielding

$$X_0^c = 4.16\frac{1 - H_D}{D_P}. \tag{4}$$

We now verify that the updated form of $X_0^c$ accurately captures the RBC partitioning from the fully resolved simulations. Figure 1g shows that Eq. (4) does not perfectly capture the analytically calculated value of $X_0^c$. However, Fig. 1h shows that the haematocrit in the child branches, the desired output of the model, is well predicted by the updated term $X_0^c$ with an $R^2$ value of 0.96, and fits the data much better than the original model, with an $R^2$ value of 0.81.

**Vessel compression reduces haematocrit and increases haematocrit heterogeneity**. We start by investigating how the compressed vessels alter the distribution of RBCs, and therefore haematocrit, at a network level. We run the network model for blood flow in an artificially generated network, shown in Fig. 2a where we treat the vessels in red as being compressed according to the description in Table 1, which for the control case implies all the vessels in the network are treated as uncompressed.

Figure 2 b shows that, when the vessels are treated with the fully compressed model (IR+AP model), there is a reduction in the average haematocrit of the compressed vessels (red distribution in the Figure) compared to the control from 19.2% to 8.8%. Figure 2b also shows that the distribution of haematocrit within the compressed vessels is wider, and has an interquartile range of [17.4%, 21.1%] in the control changing to an interquartile range of [0.9%, 13.1%] in the fully compressed case, which also becomes bimodal (HDS $p$-value < 0.05). The frequency of vessels with 0% haematocrit is increased from 1 vessel in the control case to 11 vessels in the fully compressed case.

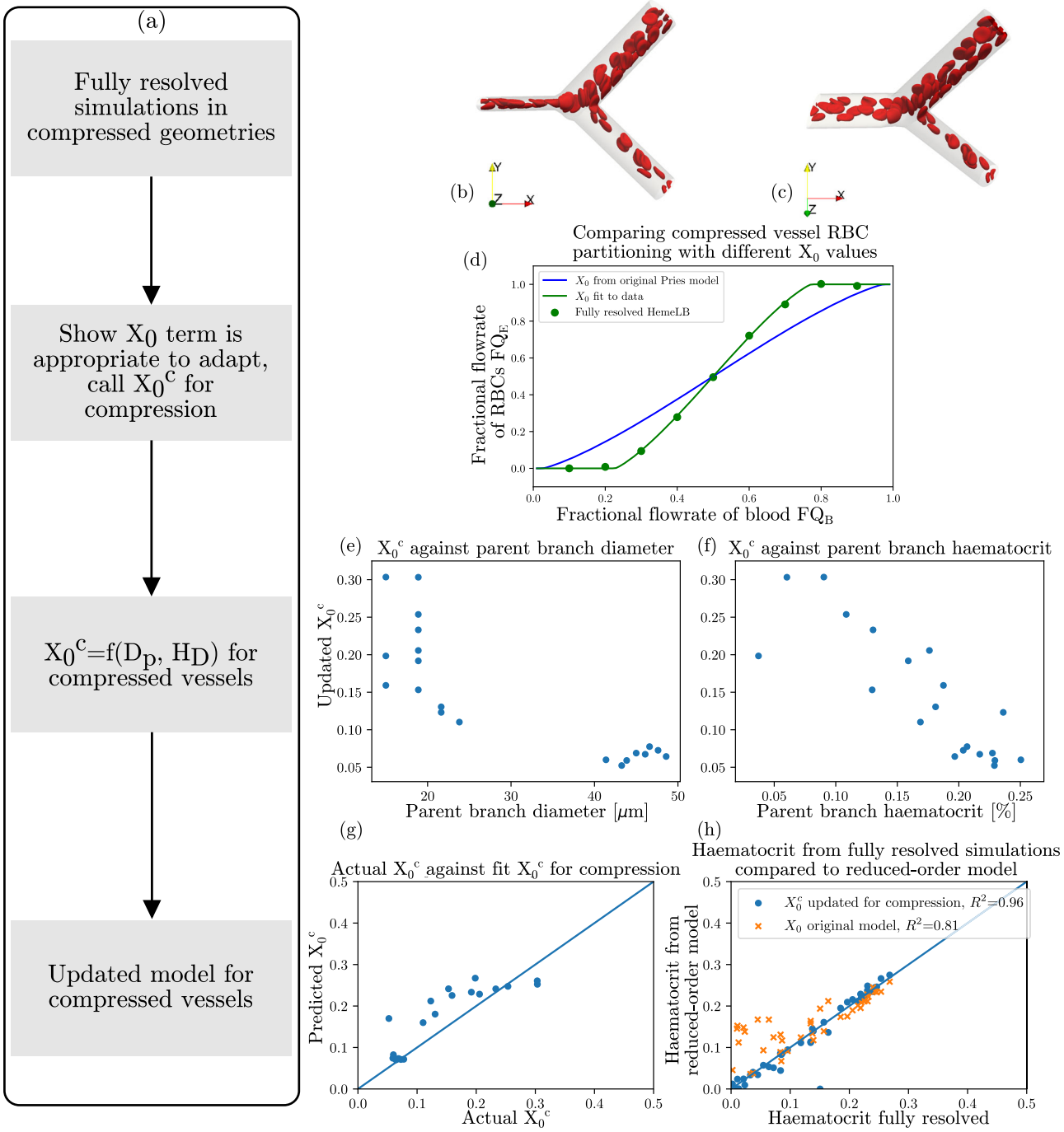


**Fig. 1 Updating the reduced-order model for compression. a** Flow chart of the process to calculate the values for $X_0^c$ for RBC partitioning in compressed vessels. **b** Snapshot of a fully resolved cellular blood flow simulation. **c** Rotated snapshot of the same simulation to show compression has an elliptical cross-section. **d** Plasma skimming curve. Green points are from varying the flow ratio in a bifurcation geometry of 33 μm with a compression before the bifurcation and an inlet haematocrit of 20%. Compares how well the original phase separation empirical model works (blue line) and how changing solely $X_0$ improves the fit (green line). $X_0$ for the green line is obtained through a fit to the data using the non-linear least-squares method. **e** $X_0^c$ calculated from fully resolved simulations with Eq. (1) against the parent branch diameter prior to deformation. **f** $X_0^c$ calculated from fully resolved simulations with Eq. (1) against the parent branch haematocrit prior to deformation. **g** Predicted $X_0^c$ from Eq. (4) against actual $X_0^c$ as calculated from fully resolved simulations. **h** Predicted haematocrit (using updated $X_0^c$ in blue and original $X_0$ in orange) against the fully resolved haematocrit. The diagonal line in **g** and **h** is a visual aid to see how close the predicted values are to the values obtained from fully resolved simulations.

Next, we separately investigate the effects of increased resistance and abnormal partitioning. When comparing the cases with increased resistance and the control cases, one initially sees that the compressed vessel (red in the Figure) distribution remains unimodal (HDS $p$-value > 0.05) with a longer tail, Fig. 2b. Contrarily, the distribution of the case with abnormal partitioning is bimodal (HDS $p$-value < 0.05). This bimodal distribution indicates that the increased heterogeneity of compressed vessel haematocrit results from abnormal partitioning of RBCs, rather than from increased resistance.

Finally, one sees that both the cases with increased resistance and abnormal partitioning reduce the compressed vessel average

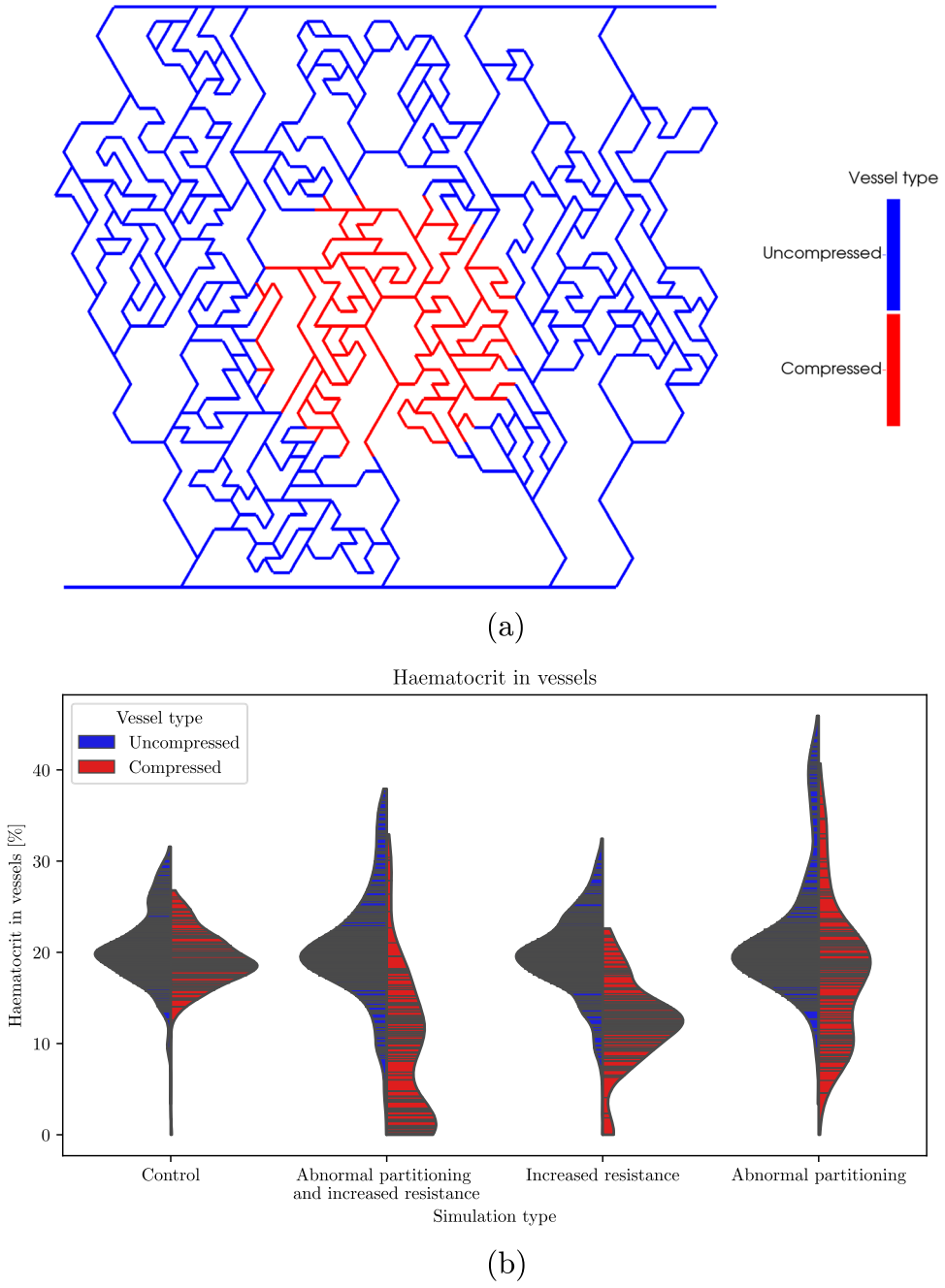


**Fig. 2 Microvascular network and effect of compression on vessel haematocrit distribution. a** Depiction of the network in which the blood flow simulations are performed. The blue vessels are treated as normal (uncompressed) blood vessels, the red vessels are treated as compressed vessels, also called compressed regions. The inlet is at the bottom left, and the outlet is at the top right. **b** Violin plots of haematocrit distribution within the vessel network. Blue and red lines correspond to blue and red vessels in **a**, respectively. The `control' case treats all vessels as normal vessels. The 'abnormal partitioning and resistance' case treats compressed vessels as having an increased resistance and abnormal partitioning. The 'abnormal partitioning' case treats compressed vessels as having just abnormal partitioning. The `resistance' case treats compressed vessels as having just increased resistance. See Table 1 for further details about the four cases. The violin plots contain the individual data points in the distribution, displayed as black lines.

haematocrit in the compressed region down to 12.1% and 17.7%, respectively, compared to 19.2% in the control. The interquartile range is also wider in the abnormal partitioning case, with a range of [10.9%, 21.2%], compared to the increased resistance case, [9.4%, 14.3%]. This finding suggests that there are two separate mechanisms that contribute to the reduction of average haematocrit in the compressed region of the network. We will investigate those mechanisms in the next sections.

**Mechanism that reduces haematocrit due to increased resistance**. Next, we explain the mechanism through which increased flow resistance of the compressed vessels reduces the haematocrit within the compressed region. We hypothesise that this effect results from diverting flow away from the compressed vessels due to their higher resistance to flow, according to Poiseuille's law. Therefore, as the phase separation effect disproportionally favours RBC flow into the higher-flowing child branch[11], RBC

**Table 1 Summary of simulation cases.**

| Name | Description | Flow Solver | Phase separation model |
|---|---|---|---|
| Control case | Vessels are treated as non-compressed for control | Supplementary Eq. (1), Poiseuille circular | Supplementary Eqs. (7)–(9) |
| Increased resistance and abnormal partitioning case (IR+AP), fully compressed model | Vessels are treated as having an increased resistance due to reduced cross-section, and abnormal partitioning at bifurcations | Supplementary Eq. (2), Poiseuille elliptical | Updated as part of results |
| Increased resistance case (IR) | Vessels are just treated as having an increased resistance due to reduced cross-section | Supplementary Eq. (2), Poiseuille elliptical | Supplementary Eqs. (7)–(9) |
| Abnormal partitioning case (AP) | Vessels are just treated as having abnormal partitioning at bifurcations | Supplementary Eq. (1), Poiseuille circular | Updated as part of results |

Four possible scenarios for how vessels are treated in network simulations, which determine how the compressed vessels, in red in Supplementary Fig. 3, are treated.

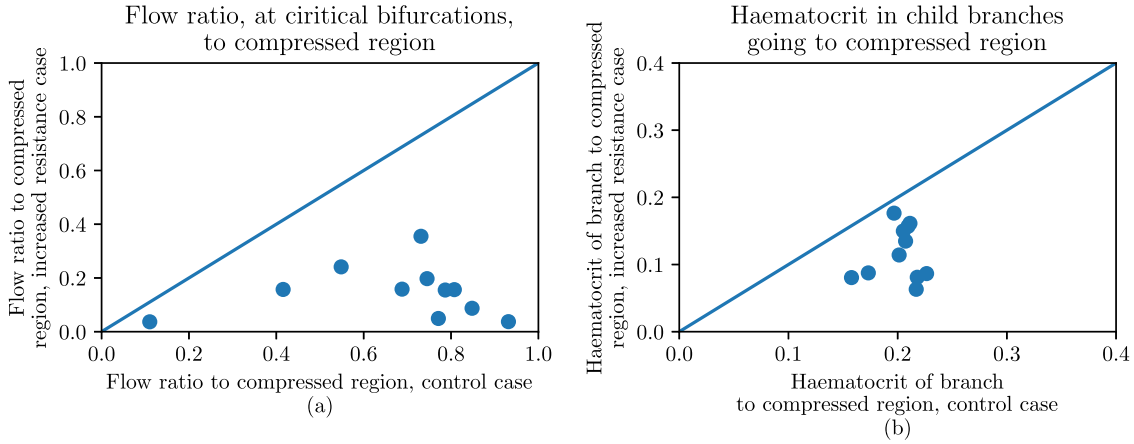


**Fig. 3 Mechanism for the effect of increased resistance on haematocrit in networks.** Effect of increased resistance at all 11 critical bifurcations in the vascular network (see Fig. 2 for network map). **a** Comparison of the flow ratio into the compressed region between the control case and the case with increased resistance, showing a reduced flow ratio into the compressed region when compressed vessels have increased resistance. **b** Comparison of the haematocrit of the child branch going into the compressed region between the control case and the case with increased resistance, showing a reduced haematocrit in the branch flowing into the compressed region when there is increased resistance. The diagonal line in **a** and **b** is a visual aid to see how close the values in the case of increased resistance are to the control case.

flow into the compressed region should be disproportionally reduced, thus decreasing the haematocrit in the compressed region.

To test our hypothesis, we define and identify 11 critical bifurcations in the network (see Methods and Supplementary Note 3 for details). As critical bifurcations are the bifurcations separating the flow going through the compression from the flow that can also go outside the compression, they allow us to test this hypothesis. We compare the flow ratio at these critical bifurcations between the control case and the case with increased resistance. Figure 3a shows that the flow ratio in the case with increased resistance is always reduced in the child branch which necessarily goes through the compressed region. This observation confirms that flow is diverted away from the compressed region.

Finally, we show how, as the critical bifurcations divert flow away from the compressed region, there is a reduction in haematocrit in the compressed region. We take the geometrical properties of the critical bifurcations and consider the haematocrit of the parent branch as obtained from the network simulations using the case with increased resistance. We then solve for the haematocrit distributions in the child branches of the critical bifurcations using the original phase separation model which contains the plasma skimming effect[11]. We prescribe the flow ratios in the child branches with and without the increased resistance and compare the resulting haematocrit distributions. Figure 3b shows that the haematocrit of the vessel going into the compressed region is smaller for the case with increased resistance as compared to the control for all critical bifurcations, which confirms our hypothesis.

**Mechanism that reduces haematocrit due to abnormal RBC partitioning**. As a next step, we investigate the effect that the abnormal partitioning has on haematocrit within the network. To this end, we use the model for abnormal partitioning which increases haematocrit heterogeneity in the child branches. We hypothesise that the reduced average haematocrit in the compressed region caused by abnormal partitioning alone is due to an enhanced network Fåhraeus effect. The network Fåhraeus effect contributes to the reduction of average haematocrit at each successive bifurcation as the average haematocrit of the two child branches at a bifurcation is lower than the haematocrit of the parent branch[20].

To investigate the hypothesis, we establish that, at a vascular bifurcation where the higher flowing child branch is disproportionately enriched in haematocrit, the average haematocrit of the child branches is equal to or lower than that of the parent branch (branch 0):

$$\overline{H}_{\text{child}} \le H_0. \tag{5}$$

Supplementary Note 4 shows how to obtain this relation. We further define $\Delta H_1$ and $\Delta H_2$ as the differences in haematocrit between the parent branch and the two child branches (branches

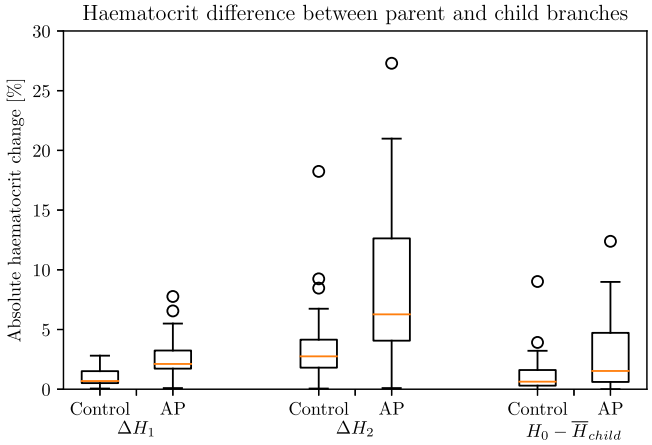


**Fig. 4 Mechanism for the effect of abnormal partitioning on haematocrit in networks.** $\Delta H_1$ and $\Delta H_2$: enrichment and impoverishment of the compressed vessels, for the control case and the case with abnormal partitioning (AP). $H_0 - \overline{H}_{\text{child}}$: reduction in average haematocrit between the parent branch and the average of the child branches, at a diverging bifurcation in the compressed region for the control case and the AP case. The box plot shows the range from the lower to the upper quartile, and the individual plotted points are outliers.

1 and 2, where branch 1 is enriched):

$$\Delta H_1 = H_1 - H_0 \geq 0, \quad \Delta H_2 = H_0 - H_2 \geq 0. \tag{6}$$

Figure 4 shows the data from diverging bifurcations in the compressed portion of the network for the control case and the case with abnormal partitioning. It can be seen that $\Delta H_1$ and $\Delta H_2$ are larger in the case with abnormal partitioning compared to the control case. Further, the mean reduction in haematocrit, $H_0 - \overline{H}_{\text{child}}$, is increased in the case with abnormal partitioning compared to the control case. Thus, a stronger network Fåhraeus effect occurs in the case of abnormal partitioning. Additionally, the enhanced heterogeneity in haematocrit due to the abnormal partitioning suffices to explain the wider and bimodal distribution of haematocrit within the compressed portion of the network observed in Fig. 2.

**Network conditions for haemodilution**. Finally, we investigate under what conditions networks are susceptible to haemodilution when vessel compression is present. We perform a parameter sweep over a wide range of inlet haematocrits to the network, from 2.5% to 30% in steps of 2.5%, and over the entire range of fraction of compressed vessels, using the fully compressed model (increased resistance and abnormal partitioning). As described in the "Methods" section and in Supplementary Fig. 3, we consider two models for the fraction of compressed vessels in a network, one where the more central vessels are compressed (radial model), and the other where random vessels are compressed (random model).

Figure 5a shows the fraction of haemodiluted vessels in the radial model. The results show that haemodilution generally increases with the fraction of compressed vessels and with a decreasing inlet haematocrit. Figure 5a also indicates that, although haemodilution is experienced over the entire parameter range, it is most pronounced when the inlet haematocrit to the network is relatively small, below 15%. In addition, this haemodilution effect is observed over a wide range of fractions of compressed vessels, suggesting that a low fraction of compressed vessels is sufficient for the network to experience haemodilution. The random model shows, Fig. 5b, that the overall haemodilution trend is not very different compared to the radial model of compressed vessels, although the haemodilution is less pronounced. Finally, we highlight that while Fig. 5 shows the fraction of haemodiluted vessels, there are also some vessels that are enriched in haematocrit due to the redistribution of red blood cells in the networks.

We also observe from Fig. 5 that the highest fraction of haemodiluted vessels is not when the fraction of compressed vessels is highest. Indeed, beyond a fraction of compressed vessels of around 80%, haemodilution decreases again. We attribute this behaviour to the mechanism for haematocrit reduction in the networks. We previously identified that increased vessel resistance has the most pronounced effect on haematocrit reduction and that it depends on flow redirection. However, when a high fraction of the network is compressed, the opportunity for flow redirection is reduced, leading to a decrease in the effect of flow resistance within the network, thus reducing the effect of compression on haemodilution.

## Discussion

Vessel compression in solid tumours is associated with both tumour tissue hypoxia and reduced survival rates in patients. Conversely, pharmacological decompression of vessels has been shown to lead to an improvement in survival rates[10]. However, a complete description of the biophysical processes underpinning these associations, particularly in relation to oxygen transport, remains elusive. Gaining a mechanistic understanding of them may uncover novel therapeutic strategies[21]. In this study, we numerically investigate RBC distribution in partially compressed vascular networks, as a model of tumour blood flow. We start by deriving a reduced-order model for RBC partitioning at bifurcations in the presence of vessel compression. We next demonstrate that vessel compression both reduces average haematocrit and increases haematocrit heterogeneity throughout the network. We identify two mechanisms that synergise non-linearly leading to this effect. The first is increased vessel resistance, and therefore flow and haematocrit diversion, in the portion of the network undergoing compression; the second is abnormal RBC partitioning in the compressed bifurcations, which underpins haematocrit heterogeneity at a network level. Finally, we show that haematocrit reduction due to compressed vessels increases with reducing inlet haematocrit to the network and with an increased fraction of compressed vessels, with a maximum of around 80% of compressed vessels.

There are several implications of the research in this work. Firstly, it provides a theoretical underpinning to explain reports from the literature, where animal models are shown to have higher tissue hypoxia and tissue oxygen heterogeneity when vessels are compressed[10], as well as the presence of plasma channels in tumour vessels[22]. We highlight the role of RBC transport at the network level in the emergence of these phenomena. The results support the hypothesis from our previous work[14] stating that, in a few successive bifurcations, vessels can be depleted of RBCs as a consequence of vessel compression[14], leading to plasma channels[22].

Secondly, this work forms part of a larger corpus in the literature studying how tumour vascular abnormalities affect blood transport in tumour microvascular networks[13,14,23–26]. Previously, inter-bifurcation distance and increased vessel diameter have been studied in isolation[13,14,23–26], and this work studies vessel compression. However, future work is necessary to identify the relative effect on blood flow, and tissue oxygenation, of the different structural abnormalities as well as their relevance in vivo. Identifying the most relevant structural abnormalities in tumour microvascular networks could open novel avenues for diagnosis and patient treatment planning[27]. Prognosis could be improved through phenotyping tumour vascular networks based

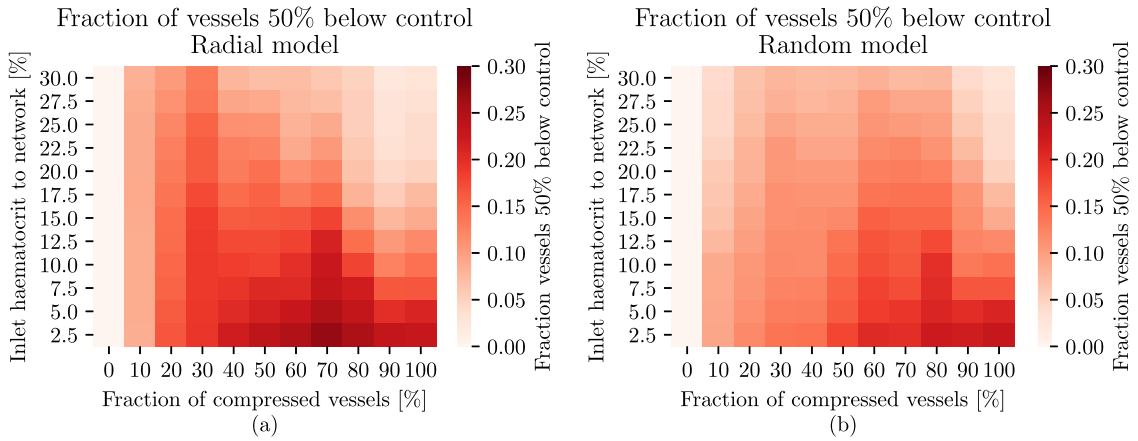


**Fig. 5 Heat maps for vessel haemodilution conditions in compressed network.** Heat map showing the fraction of haemodiluted vessels in the network for varying inlet haematocrit and fraction of compressed vessels in the network. Haemodiluted vessels are defined as vessels with a haematocrit of less than half of the haematocrit of the same vessel in the control case. **a** Radial model for the network, **b** random model for the network. See Supplementary Fig. 3 for an illustration of the radial and random models.

on their structural abnormalities, as these correlate with survival rates[8]. Treatment planning could be improved through optimising treatment based on the present structural abnormalities, to improve treatment delivery or efficacy[28,29].

Thirdly, the results support the notion, hypothesised in our previous work[14], that healthy vascular networks are protected against the effects of naturally occurring structural abnormalities for as long as their average haematocrit remains high. Diseased networks, however, are susceptible to a positive feedback loop whereby they are at a higher risk of haemodilution as they have lower average haematocrit than healthy networks[22].

## Methods

Blood is modelled in two different ways. The first method is more accurate at a high computational cost, whereas the other method is based on a more efficient reduced-order model. The former, more highly resolved simulations serve to inform the latter reduced-order model.

**Particulate blood flow**. With the first method, we treat blood as a suspension of deformable RBCs in a continuous plasma phase. The plasma is assumed to be a continuous Newtonian fluid, and the viscoelastic properties of plasma are not a leading-order effect in the regime investigated[30]. The non-Newtonian behaviour of blood arises from the presence of the deformable RBCs which are modelled as hyperelastic membranes.

The physics of the particulate blood flow is characterised by the Reynolds number and the capillary number. The Reynolds number quantifies the ratio of inertial to viscous forces in fluid flow. The capillary number quantifies the deformability of the particles, where higher capillary numbers correspond to softer particles. The Reynolds and capillary numbers are defined as[31]

$$\mathrm{Re} = \frac{\rho u_{\max} D}{\mu}, \quad \mathrm{Ca} = \frac{\mu \dot{\gamma} r_{\mathrm{RBC}}}{\kappa_s} \tag{7}$$

where $\rho$ is the fluid density, $u_{\max}$ is the maximum velocity in the channel, $D$ is the channel diameter, $\mu$ is the dynamic viscosity of the suspending fluid, $\dot{\gamma}$ is a typical shear rate in the system, $r_{\mathrm{RBC}}$ is the rest radius of the RBC, and $\kappa_s$ is the elastic modulus of the RBC. In our simulations, the Reynolds and capillary numbers are set to 0.5 and 0.1, respectively[14].

The algorithm for solving for particulate blood flow is implemented in the open-source software HemeLB (https://github.com/hemelb-codes/hemelb)[32]. Additional information on the model and the numerical scheme can be found in Supplementary Note 5 and the references therein.

**Network blood flow**. With the second method, blood flow is treated in a one-dimensional network model imposing Poiseuille's law on each vessel segment, with additional components to the model accounting for the Fåhraeus effect, the Fåhraeus–Lindqvist effect, and partitioning of RBCs at bifurcations[19]. Additional information on the model and numerical scheme can be found in Supplementary Note 1 and the references therein.

**Artificial network generation**. The networks are generated using the open-source software Tumorcode[33–35]. It uses an algorithm to randomly generate vessel networks on a mesh. The algorithm is based on Murray's law and geometrical properties for capillaries, arterioles, and venules. Tumorcode also has the ability to reproduce the evolution of a tumour vessel network in the in silico-generated vascular network. However, for the purpose of the research here only the healthy networks are used, to isolate the network from other structural abnormalities. An example of a generated network is depicted in Fig. 2a. We use the two-dimensional default network generator, with a single inlet and a single outlet. The single inlet and outlet facilitate the choice of boundary conditions, with the inlet set as a flowrate and the outlet as a pressure of zero. As there is a single inlet and outlet, the absolute value of the flowrate does not have an effect on the haematocrit output of the simulations. Unless stated otherwise, the inlet haematocrit is 20% The two-dimensional networks are generated within a square surface of 5000 μm by 5000 μm.

Within the network, we treat some vessels differently, detailed in Table 1, which we call the compressed vessels or compressed regions. Initially, the compressed vessels are in the centre of the network and are vessels that have both ends within a 1000 $\mu$m radius of the centre of the vessel network. We also vary the fraction of compressed vessels, using a radial model and a random model, see Supplementary Note 6. The radial model is a model for tumours where the solid stress is higher in the centre, thereby compressing vessels more in the centre of the tumour[36]. In the radial model, the compressed vessels are the vessels closest to the centre of the network (see Supplementary Fig. 3a–f). The random model is an alternative model where compressed vessels are not deterministically situated. In the random model, a random selection of vessels is compressed to reach the desired fraction of total vessels (see Supplementary Fig. 3g–l).

**Processing results**. The average haematocrit values reported are calculated as follows:

$$\overline{H} = \frac{1}{n}\sum_{i=1}^{n} H_i, \tag{8}$$

where $\overline{H}$ is the average discharge haematocrit, $n$ is the number of vessels, and $H_i$ is the discharge haematocrit of the $i$th vessel.

Hartigan's dip statistic (HDS) is used to test for the unimodality of a distribution[37]. The null hypothesis of the test is that the distribution is unimodal. If the null hypothesis is rejected, that is the p-value from the test is below 0.05, the distribution is multimodal, and we determine how many modes there are based on the number of peaks in the distribution.

To process the results, we also define a set of critical bifurcations, see Supplementary Note 3. A critical bifurcation is defined as a diverging bifurcation where

1. one of the child branches has every possible path emanating from it going through the compressed region and
2. the other child branch has at least one path emanating from it not going through the compressed region.

The critical bifurcations are therefore the bifurcations in the network that separate flow going through the compressed region from the flow that can go outwith the compressed region. Supplementary Fig. 1 illustrates one of these critical bifurcations, and the remaining 10 are available from the downloadable supplementary material.

In addition, to quantify the effect that vessel compression has on the reduction of haematocrit in the networks, we define a metric which is a proxy to quantify haematocrit reduction in a network. The metric uses the basic form

$$F_{\mathrm{hdil}} = \frac{N_{\mathrm{hdil}}}{N_{\mathrm{tot}}}, \tag{9}$$

where $F_{\mathrm{hdil}}$ is the fraction of haemodiluted vessels in the network, $N_{\mathrm{hdil}}$ is the number of haemodiluted vessels in the network, and $N_{\mathrm{tot}}$ is the total number of vessels in the network. The condition for haemodilution is that the haematocrit in a given vessel has a relative value of 50% or less of the haematocrit of the same vessel in the control case.

## Data availability

The result of the simulation showing the critical bifurcations and flow path has been deposited in Edinburgh DataShare (https://doi.org/10.7488/ds/7544).

## Code availability

The code used for the simulations and data analysis is available from the corresponding authors upon reasonable request.

Received: 15 June 2023; Accepted: 20 December 2023;
Published online: 05 February 2024

## References

1. Jain, R. K., Martin, J. D. & Stylianopoulos, T. The role of mechanical forces in tumor growth and therapy. *Annu. Rev. Biomed. Eng.* **16**, 321–346 (2014).
2. Brizel, D. M. et al. *Tumor Oxygenation Predicts for the Likelihood of Distant Metastases in Human Soft Tissue Sarcoma* 1. Technical Report. http://aacrjournals.org/cancerres/article-pdf/56/5/941/2952197/cr0560050941.pdf (1996).
3. Brown, J. M. & Wilson, W. R. Exploiting tumour hypoxia in cancer treatment. *Nat. Rev. Cancer* **4**, 437–447 (2004).
4. Jain, R. K. Normalizing tumor microenvironment to treat cancer: bench to bedside to biomarkers. *J. Clin. Oncol.* **31**, 2205–2218 (2013).
5. Martin, J. D., Cabral, H., Stylianopoulos, T. & Jain, R. K. Improving cancer immunotherapy using nanomedicines: progress, opportunities and challenges. *Nat. Rev. Clin. Oncol.* **17**, 251–266 (2020).
6. Munn, L. L. & Jain, R. K. Vascular regulation of antitumor immunity. *Science* **365**, 544–545 (2019).
7. Padera, T. et al. Cancer cells compress intratumour vessels. *Nature* **427**, 695 (2004).
8. Fang, L. et al. Flattened microvessel independently predicts poor prognosis of patients with non-small cell lung cancer. *Oncotarget* **8**, 30092–30099 (2017).
9. Hagendoorn, J. et al. Onset of abnormal blood and lymphatic vessel function and interstitial hypertension in early stages of carcinogenesis. *Cancer Res.* **66**, 3360–3364 (2006).
10. Chauhan, V. P. et al. Angiotensin inhibition enhances drug delivery and potentiates chemotherapy by decompressing tumour blood vessels. *Nat. Commun.* **4**, 2516 (2013).
11. Secomb, T. W. Blood Flow in the Microcirculation. *Annu. Rev. Fluid Mech.* **49**, 443–461 (2017).
12. Rashidi, Y. et al. Red blood cell lingering modulates hematocrit distribution in the microcirculation. *Biophys. J.* **122**, 1526–1537 (2023).
13. Bernabeu, M. O. et al. Abnormal morphology biases hematocrit distribution in tumour vasculature and contributes to heterogeneity in tissue oxygenation. *Proc. Natl Acad. Sci. USA* **117**, 27811–27819 (2020).
14. Enjalbert, R., Hardman, D., Krüger, T. & Bernabeu, M. O. Compressed vessels bias red blood cell partitioning at bifurcations in a hematocrit-dependent manner: implications in tumor blood flow. *Proc. Natl Acad. Sci. USA* **118**, https://doi.org/10.1073/pnas.2025236118 (2021).
15. Goldman, D. Theoretical models of microvascular oxygen transport to tissue. *Microcirculation* **15**, 795–811 (2008).
16. Jain, R. K. Determinants of tumor blood flow: a review. *Cancer Res.* **48**, 2641–2658 (1988).
17. Seano, G. et al. Solid stress in brain tumours causes neuronal loss and neurological dysfunction and can be reversed by lithium. *Nat. Biomed. Eng.* **3**, 230–245 (2019).
18. Pries, A., Ley, K., Classen, M. & Gaehtgens, P. Red Cell Distribution at Microvascular. *Microvasc. Res.* **38**, 81–101 (1989).
19. Pries, A. R., Secomb, T. W., Gaehtgens, P. & Gross, J. F. Blood flow in microvascular networks. Experiments and simulation. *Circ. Res.* 826–834 https://www.ncbi.nlm.nih.gov/pubmed/2208609 (1990).
20. Pries, A. R., Ley, K. & Gaehtgens, P. Generalization of the Fahraeus principle for microvessel networks. *Am. J. Physiol.—Heart Circ. Physiol.* **251**, H1324-1332 (1986).
21. Nia, H. T., Munn, L. L. & Jain, R. K. Physical traits of cancer. *Science* **370**, eaaz0868 (2020).
22. Kamoun, W. S. et al. Simultaneous measurement of RBC velocity, flux, hematocrit and shear rate in vascular networks. *Nat. Methods* **7**, 655–660 (2010).
23. Merlo, A. et al. A few upstream bifurcations drive the spatial distribution of red blood cells in model microfluidic networks. *Soft Matter* **18**, 1463–1478 (2022).
24. Sweeney, P. W., D'Esposito, A., Walker-Samuel, S. & Shipley, R. J. Modelling the transport of fluid through heterogeneous, whole tumours in silico. *PLoS Comput. Biol.* **15**, e1006751 (2019).
25. d'Esposito, A. et al. Computational fluid dynamics with imaging of cleared tissue and of in vivo perfusion predicts drug uptake and treatment responses in tumours. *Nat. Biomed. Eng.* **2**, 773–787 (2018).
26. Welter, M., Fredrich, T., Rinneberg, H. & Rieger, H. Computational model for tumor oxygenation applied to clinical data on breast tumor hemoglobin concentrations suggests vascular dilatation and compression. *PLoS ONE* **11**, 1–42 (2016).
27. Dewhirst, M. W., Mowery, Y. M., Mitchell, J. B., Cherukuri, M. K. & Secomb, T. W. Rationale for hypoxia assessment and amelioration for precision therapy and immunotherapy studies. *J. Clin. Investig.* **129**, 489–491 (2019).
28. Dewhirst, M. W. & Secomb, T. W. Transport of drugs from blood vessels to tumour tissue. *Nat. Rev. Cancer* **17**, 738–750 (2017).
29. Jain, R. K. Normalization of tumor vasculature: an emerging concept in antiangiogenic therapy. *Science* **307**, 58–62 (2005).
30. Varchanis, S., Dimakopoulos, Y., Wagner, C. & Tsamopoulos, J. How viscoelastic is human blood plasma? *Soft Matter* **14**, 4238–4251 (2018).
31. Krüger, T., Varnik, F. & Raabe, D. Efficient and accurate simulations of deformable particles immersed in a fluid using a combined immersed boundary lattice Boltzmann finite element method. *Comput. Math. Appl.* **61**, 3485–3505 (2011).
32. Mazzeo, M. D. & Coveney, P. V. HemeLB: a high performance parallel lattice-Boltzmann code for large scale fluid flow in complex geometries. *Comput. Phys. Commun.* **178**, 894–914 (2008).
33. Rieger, H. & Welter, M. Integrative models of vascular remodeling during tumor growth. *Wiley Interdiscip. Rev.: Syst. Biol. Med.* **7**, 113–129 (2015).
34. Fredrich, T., Welter, M. & Rieger, H. Tumorcode: a framework to simulate vascularized tumors. *Eur. Phys. J. E* **41**, 55 (2018).

35. Rieger, H., Fredrich, T. & Welter, M. Physics of the tumor vasculature: Theory and experiment. *Eur. Phys. J.* **131**, 1–24 (2016).
36. Stylianopoulos, T. et al. Coevolution of solid stress and interstitial fluid pressure in tumors during progression: Implications for vascular collapse. *Cancer Res.* **73**, 3833–3841 (2013).
37. Hartigan, J. A. & Hartigan, P. M. The dip test of unimodality. *Ann. Stat.* **13**, 70–84 (1985).

## Acknowledgements

We acknowledge the contributions of the HemeLB development team. Supercomputing time on the ARCHER2 UK National Supercomputing Service (http://www.archer2.ac.uk) was provided by the 'UK Consortium on Mesoscale Engineering Sciences (UKCOMES)' under EPSRC grant no. EP/R029598/1, with computational support from the 'Computational Science Centre for Research Communities (CoSeC)' through UKCOMES. M.O.B. gratefully acknowledges funding from: Fondation Leducq Transatlantic Network of Excellence (17 CVD 03); EPSRC grant no. EP/X025705/1; British Heart Foundation and The Alan Turing Institute Cardiovascular Data Science Award (C-10180357); Diabetes UK (20/0006221); Fight for Sight (5137/5138); the SCONe projects funded by Chief Scientist Office, Edinburgh & Lothians Health Foundation, Sight Scotland, the Royal College of Surgeons of Edinburgh, the RS Macdonald Charitable Trust, and Fight For Sight; the Neurii initiative which is a partnership among Eisai Co., Ltd, Gates Ventures, LifeArc and HDR UK. R.E. gratefully acknowledges his funding as part of a Fondation Leducq Transatlantic Network of Excellence (17 CVD 03, https://www.mdc-berlin.de/leducq-attract), EPSRC grant no. EP/X025705/1, and The University of Edinburgh through a Chancellor's Fellow PhD studentship. For the purpose of open access, the authors have applied a Creative Commons Attribution (CC BY) licence to any Author Accepted Manuscript version arising from this submission.

## Author contributions

R.E., T.K. and M.O.B. designed research; R.E. performed research; R.E., T.K. and M.O.B. analysed data; R.E., T.K. and M.O.B. wrote the paper.

## Competing interests

The authors declare no competing interests.

## Additional information

**Supplementary information** The online version contains supplementary material available at https://doi.org/10.1038/s42005-023-01510-8.

**Correspondence** and requests for materials should be addressed to Timm Krüger or Miguel O. Bernabeu.

**Peer review information** *Communications Physics* thanks the anonymous reviewers for their contribution to the peer review of this work.

**Reprints and permission information** is available at http://www.nature.com/reprints

**Publisher's note** Springer Nature remains neutral with regard to jurisdictional claims in published maps and institutional affiliations.